

Catalytic Activity of Single-Atom Copper Modified Reconstructed Cerium Dioxide (100) Surface for Ammonia Oxidation: A DFT+U Study

Jiajie Du and Xueqing Gong*

State Key Laboratory of Synergistic Chem-Bio Synthesis, School of Chemistry and Chemical Engineering, Shanghai Jiao Tong University, Shanghai 200240, China.

*Corresponding author: xqgong@sjtu.edu.cn

Received on 12 February 2025; accepted on 27 March 2025

Abstract

Ammonia has been proposed as a potential carbon-free energy source. However, a highly active catalyst is required for ammonia oxidation to promote the combustion rate. In this study, the single-atom copper catalyst loaded on the reconstructed cerium dioxide (100) surface with the pocket-like structure ($\text{Cu}_1/\text{CeO}_4\text{-t-p}$) is constructed for ammonia oxidation, and the catalytic process is investigated using the density functional theory calculations corrected by on-site Coulomb interactions (DFT+U). The adsorptions of ammonia and oxygen, the dissociation of ammonia and the oxidation of the dissociated ammonia species are systematically examined.

Key words: ammonia oxidation, reconstructed cerium dioxide (100) surface, single-atom copper catalyst, density functional theory.

1. Introduction

Cerium dioxide (CeO_2) has been widely used in many important catalytic reactions like CO oxidation [1] and water-gas shift reaction [2]. It is generally believed that the excellent catalytic performance of CeO_2 is related to the highly localized 4f orbital of the Ce elements and the remarkable activity of the lattice oxygen [3]. Among the various low-index surfaces of cerium dioxide, experimental studies have shown that the $\text{CeO}_2(100)$ surface has higher reactivity and oxygen storage capacity than its (110) and (111) counterparts [4, 5]. Notably, $\text{CeO}_2(100)$ is a common polar surface with high surface energy, which often undergoes the reconstruction to increase the surface stability. The scanning tunneling microscopy (STM) and high-resolution transmission electron microscopy (HRTEM) studies have revealed that the exposed (100) surface at CeO_2 nanocubes is not fully cerium or oxygen terminated [6]. The theoretical work conducted by Capdevila-Cortada *et al.* [7] showed that the $\text{CeO}_2(100)$ surface with CeO_4 termination ($\text{CeO}_4\text{-t}$) has lower surface energy than the oxygen (O-t) or cerium termination (Ce-t). Zhou *et al.* [8] have proposed a series of more stable reconstructed $\text{CeO}_4\text{-t}$ $\text{CeO}_2(100)$ surfaces with pocket-like structure, and they also showed that these surfaces have superior affinity toward the adsorption and dispersion of single metal atoms.

Ammonia has been proposed as a potential carbon-free energy source due to its high energy density and zero carbon dioxide emission [9]. However, compared with common fossil fuels, the application of ammonia as fuel faces the challenges like high ignition temperature, low combustion rate and the emission of NO_x [10, 11]. Therefore, it is essential to design the catalysts for ammonia oxidation with high efficiency. At the same time, recent progresses in single-atom catalysts have drawn great attention. Various copper single-atom catalysts have been prepared and applied in many catalytic processes due to their high reactivity and selectivity [12]. Moreover, several CeO_2 supported single-atom copper catalysts have also been reported. For example, Rabee *et al.* [13] prepared the CeO_2 supported single-atom Cu catalysts modified by Fe for the reverse water gas shift reaction; Huang *et al.* [14] developed the single-atom Cu catalysts at CeO_2 for electrocatalytic reduction of CO_2 . Considering the high reactivity of $\text{CeO}_2(100)$, we expected that the excellent ammonia oxidation activity could be achieved by loading atomic copper on the $\text{CeO}_2(100)$ surface.

In the present work, we conducted the density functional theory calculations corrected by on-site Coulomb interactions (DFT+U) to systematically investigate the catalytic processes of ammonia oxidation on the single-atom copper modified reconstructed

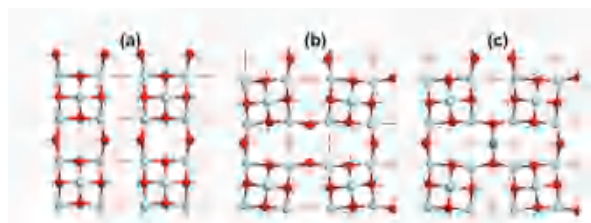


Figure 1. Top view of (a) CeO₄-t (b) CeO₄-t-p (c) Cu₁/CeO₄-t-p CeO₂(100) surfaces. Red: O; light grey: Ce; orange: Cu; blue dashed circle: CeO₄ unit.

CeO₂(100) surface. Detailed characteristics of the adsorptions and reactions within the possible ammonia oxidation pathways were carefully studied. It has been generally found that the localized 4*f* electron and the oxygen storage capacity of CeO₂ are both favorably involved in the reaction processes.

2. Computational methods and models

All the spin-polarized DFT+U calculations were carried out using Vienna *ab initio* Simulation Package (VASP) [15]. Electronic exchange and correlation were treated within the generalized gradient approximation (GGA) by using Perdew-Burke-Ernzerhof (PBE) functional [16]. The project-augmented wave method [17] with an energy cutoff of 450 eV was employed to describe the interaction between atomic cores and electrons.

Throughout all the calculations, the on-site Coulomb interaction correction with an effective *U* of 5.0 eV for Ce 4*f* orbitals was applied to describe the localized electronic states, which was consistent with our previous study [8]. The transition states (TS) were located by a constrained optimization method [18] and were verified when (i) all forces on the relaxed atoms vanish and (ii) the total energy is a maximum along the reaction coordination, but it is a minimum with respect to the rest of the degrees of freedom. All the calculations of structural optimization and transition states optimization were converged until the Hellman-Feynman forces on each ion were less than 0.05 eV/Å.

The lattice parameter of CeO₂ unit cell was optimized using a Γ -centered 5×5×5 *k*-point mesh, and the result of *a* = *b* = *c* = 5.486 Å was obtained, which was consistent with the experimental value [19] of *a* = *b* = *c* = 5.411 Å. For model construction, we first built the CeO₄-t surface (Figure 1a) from the *p*(4 × 4) slab cell. The clean CeO₄-t-p surface (Figure 1b) was then built by adjusting the positions of the surface O_{2c} on the CeO₄-t surface according to our previous study [8].

The model of single-atom copper catalyst (Cu₁/CeO₄-t-p, see Figure 1c) was further built by adding a copper atom into the position between two surface O_{2c} of the clean CeO₄-t-p surface. The CeO₄-t-p and the Cu₁/CeO₄-t-p surfaces were simulated with slabs containing 9 atomic layers. To prevent the interactions between the slabs, the vacuum layer of about 12 Å was set between neighboring slabs. It needs to be mentioned that the thermal stability of the single-atom Cu catalyst built in this way is also an important issue, which will be in-depth studied in our future work.

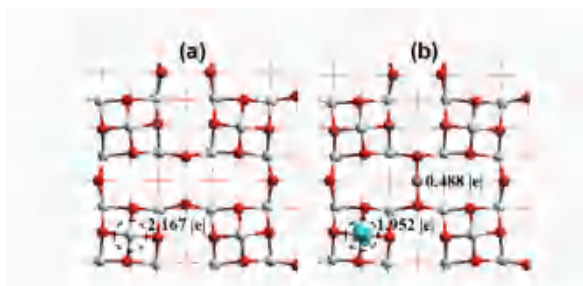


Figure 2. Calculated spin charges (top view, in blue) and Bader charges of (a) CeO₄-t-p and (b) Cu₁/CeO₄-t-p surfaces.

The adsorption energy (*E*_{ads}) of adsorbates (NH₃ and O₂) on the reconstructed CeO₂(100) surfaces was defined as:

$$E_{\text{ads}} = -(E_{\text{mol/slab}} - E_{\text{slab}} - E_{\text{mol}})$$

where *E*_{mol/slab} is the calculated energy of the surface slab with adsorbates, *E*_{slab} is the calculated energy of the clean surface slab, and *E*_{mol} is the calculated energy of the isolated molecule. The oxygen vacancy formation energy (*E*_{vac}) was defined as:

$$E_{\text{vac}} = E_{\text{slab/vac}} + 0.5 E_{\text{O}_2} - E_{\text{slab}}$$

where *E*_{slab} is the calculated energy of the clean surface slab, *E*_{slab/vac} is the calculated energy of the surface slab with a single oxygen vacancy, and *E*_{O₂} is the calculated energy of a single O₂ molecule.

3. Results and discussion

3.1 Electronic structure of CeO₄-t-p and Cu₁/CeO₄-t-p surface

To learn the effect of single-atom copper modification on the CeO₄-t-p surface, we performed the electronic structure calculation. Figure 2 shows the calculated spin charge densities and Bader charges of the CeO₄-t-p and Cu₁/CeO₄-t-p surfaces.

The existence of a localized electron at the surface CeO₄ unit was clarified by the typical charge distribution of a 4*f* electron, and the Bader charge analysis also showed that the Ce of this CeO₄ unit was reduced to Ce³⁺. In addition, the Bader charge of the anchored single Cu was calculated to be 0.488 |*e*|, which is close to that of Cu in the bulk Cu₂O (0.539 |*e*|). These results indicated that the oxidation state of Cu is +1 and the lost electron of Cu transfers to one surface Ce.

3.2 Formation of oxygen vacancies on Cu₁/CeO₄-t-p surfaces

The superior oxygen storage capacity of CeO₂ is closely related to the formation of oxygen vacancies and we systematically calculated the vacancy formation energies (*E*_{vac}) of the lattice oxygen with different coordination numbers, and the results are showed in Figure 3.

On the Cu₁/CeO₄-t-p surface, the O_{2c} (2-fold coordination O) gave very small *E*_{vac} of 1.04 eV, while the O_{3c} (3-fold coordination O) gave larger *E*_{vac} of 1.85 eV. Compared with the *E*_{vac} of O_{2c} and O_{3c} on CeO₄-t surface (1.27 and 2.06 eV, respectively) and

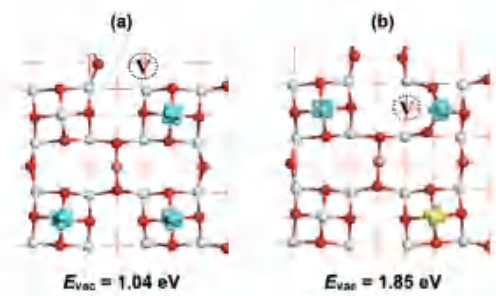


Figure 3. Calculated spin charge density (top view, in blue and yellow) and the vacancy formation energies of the Cu₁/CeO₄-t-p surface with one oxygen vacancy at (a) O_{2c} or (b) O_{3c} site. V represents the oxygen vacancy.

the E_{vac} of O_{2c} on O-t surface (2.01 eV) [20], both the E_{vac} of O_{2c} and O_{3c} on the Cu₁/CeO₄-t-p surface became smaller. Therefore, it indicates that these surface oxygens are easier to remove. Experimental studies showed that ammonia oxidation on metal oxide catalysts usually follows the Mars-van Krevelen mechanism [21]. Thus, small E_{vac} values also suggested high catalytic activities of the Cu₁/CeO₄-t-p surface.

Moreover, Figure 3 shows the calculated spin charge densities of the Cu₁/CeO₄-t-p surface with the oxygen vacancy at different sites. One can see the existence of three localized electrons at three different Ce of the surface CeO₄ units.

3.3 Oxygen adsorption

The Cu and Ce sites of the surface are the possible locations for the adsorption of oxygen (O₂). The adsorption structures and energies of one oxygen molecule on the CeO₄-t-p and Cu₁/CeO₄-t-p surfaces are shown in Figure 4a–4c.

The calculated results showed that the oxygen prefers to adsorb on the Ce site of Cu₁/CeO₄-t-p with the adsorption energy of 1.10 eV, while the adsorption energy on the Cu site is far less than the Ce site, only 0.32 eV. Interestingly, the O₂ adsorption on the Ce site of CeO₄-t-p is also weak with the adsorption energy of 0.26 eV.

Compared with the adsorption structure of oxygen on the Cu₁/CeO₄-t-p surface, the oxygen molecule adsorbed on the CeO₄-t-p surface is farther away from the Ce site. We also found that the bond length of the adsorbed oxygen on the Ce site of the Cu₁/CeO₄-t-p surface is 1.340 Å. The increased O–O bond length indicates that the oxygen is activated after adsorption.

To clarify the effect on oxygen adsorption after the loading of the single Cu atom, we performed the electronic structure analysis. Figure 4d shows the spin charge density of the surface after oxygen adsorption on the Ce site of Cu₁/CeO₄-t-p. The result showed that the localized electron at the Ce of the surface CeO₄ unit transfers to the adsorbed oxygen molecule.

The Bader charge of the whole oxygen molecule is about $-0.65 |e|$, which indicates that the adsorbed species can actually be taken as an O₂[−] species. The formation of O₂[−] will also enhance the electrostatic interaction between it and the Ce⁴⁺ below, which can rationalize the strong adsorption of oxygen on the Ce site of Cu₁/CeO₄-t-p.

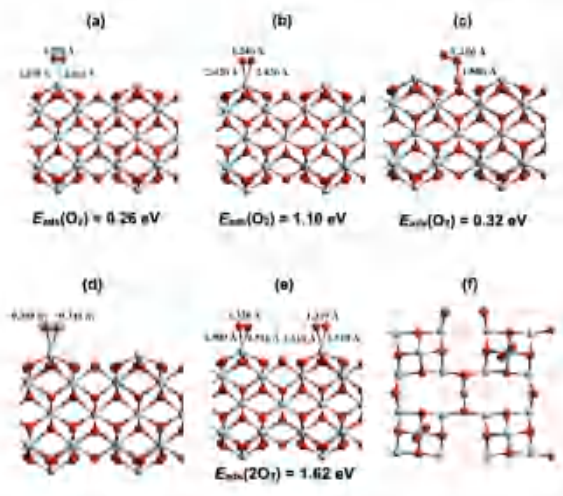


Figure 4. Calculated structures (side view) and adsorption energies of one oxygen molecule adsorbed on (a) the Ce site of CeO₄-t-p, (b) the Ce site of Cu₁/CeO₄-t-p, (c) the Cu site of Cu₁/CeO₄-t-p. (d) is the calculated spin charge density (side view, in yellow) and Bader charges of (b). (e) and (f) are the calculated structures (side and top views) of the two oxygen molecules co-adsorbed on Cu₁/CeO₄-t-p.

It needs to be mentioned that several experimental and theoretical studies reported that the absorbed oxygen is not detected on the unreduced cerium dioxide [22], which is consistent with the above calculated results.

The co-adsorption of two oxygen molecules on two different surface Ce sites was also considered (Figure 4e and 4f). The adsorption energy of the second oxygen molecule on the Ce site is rather small (about 0.52 eV), clearly due to the fact that no more localized electron can transfer to it.

3.4 Ammonia adsorption

The adsorption of ammonia is a crucial step of the ammonia oxidation. Figure 5 illustrates the calculated adsorption structures of ammonia on the CeO₄-t-p and Cu₁/CeO₄-t-p surface.

The calculated adsorption energy of ammonia on the Ce site of the CeO₄-t-p surface is 0.72 eV and the distance between Ce and N is about 2.736 Å (Figure 5a). After the single-atom copper was loaded (Figure 5b), the adsorption energy and structure of ammonia had no significant change, which indicates that the single-atom copper has little effect on the adsorption of ammonia.

The Cu site of Cu₁/CeO₄-t-p is another possible adsorption site of ammonia. There are two main adsorption structures of ammonia on the Cu sites: (1) ammonia adsorbed on the top of Cu (Figure 5c); (2) ammonia adsorbed on the side position of Cu, in which the two N–H groups of the ammonia molecule can form hydrogen bonds with the two lattice oxygens on the surface (Figure 5d and 5e). The distances between N in ammonia and Cu atoms in these two adsorption structures are around 2.25 Å. It can be seen that the adsorption structure with the tilted ammonia has a higher adsorption energy, suggesting that the hydrogen bonding is favorable for the adsorption of ammonia on the surface Cu site. However, the adsorption energies of both structures are still rather

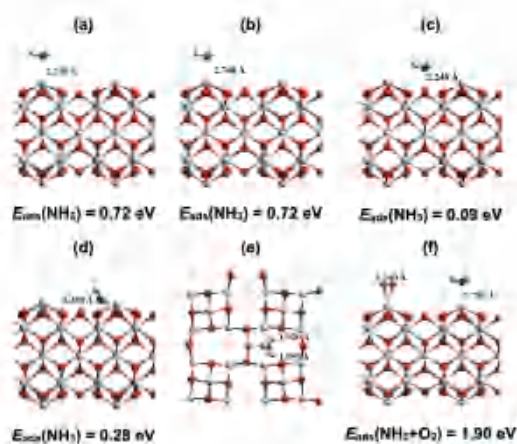


Figure 5. Calculated adsorption energies and structures of ammonia on the (a) Ce site of CeO₄-t-p, (b) Ce site of Cu₁/CeO₄-t-p, (c) top of the Cu site of Cu₁/CeO₄-t-p, (d) tilt position of the Cu site of Cu₁/CeO₄-t-p, (e) is the top view of (d), and (f) the side view of the co-adsorption structure of ammonia and oxygen. Blue: N, white: H.

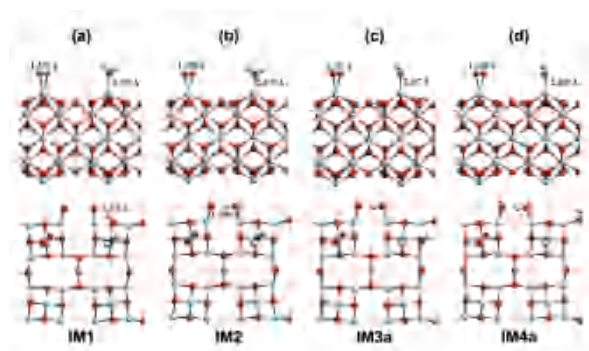


Figure 6. Calculated structures (top: side view; bottom: top view) of ammonia dissociation. (a, b) the ammonia dissociation to O_{3c} and O_{2c} to form NH₂ species, respectively. (c, d) the NH₂ species dissociation to O_{3c} and O_{2c} to form NH species, respectively.

small, indicating that the adsorption of ammonia molecules on the Cu site is weak. Therefore, ammonia is still more likely to adsorb on the Ce sites of the surface.

The co-adsorption of ammonia and oxygen was also considered, and Figure 5f illustrates the calculated adsorption energy and structure. The overall adsorption energy of ammonia and oxygen is 1.90 eV, which is larger than the adsorption energy of two oxygen molecules (1.62 eV). It indicates that the ammonia can adsorb on another Ce site after the adsorption of oxygen, *i.e.*, the ammonia and the oxygen can adsorb on two different Ce sites simultaneously.

3.5 Ammonia dissociation

The dissociation of ammonia is the first step for its activation. In Figure 6, we illustrated the calculated structures of the

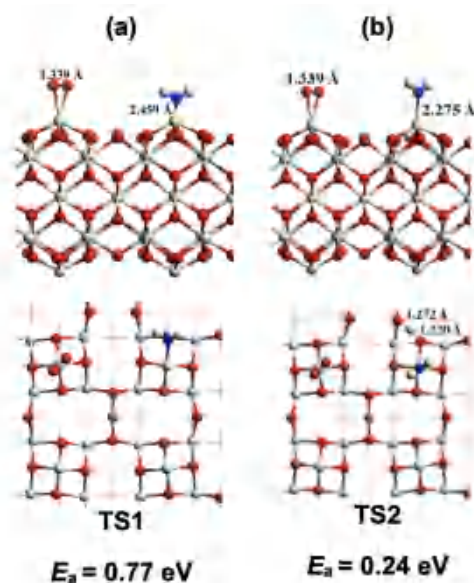


Figure 7. Calculated transition states (top and side views) and activation energies of (a) dissociation of ammonia to O_{3c} and (b) hydrogen migration.

dissociation of ammonia on the Cu₁/CeO₄-t-p surface. The results showed that the dissociation of hydrogen from the ammonia to the O_{2c} (Figure 6a) is exothermic by 0.30 eV, whereas the dissociation to O_{3c} (Figure 6b) is endothermic by 0.18 eV, suggesting that the dissociation of hydrogen from the ammonia to O_{2c} is more favorable.

Following the hydrogen dissociation to the O_{2c}, there can form a hydrogen bond with another neighboring O_{2c} with a length of about 1.8 Å. The formation of hydrogen bond can help increase the stability. While after the hydrogen dissociation to the O_{3c}, though it will also form a hydrogen bond with the adjacent O_{2c}, the length of the hydrogen bond is longer (~2.2 Å). Moreover, the dissociated hydrogen is electrostatically repulsed with the adjacent Ce, which is unfavorable for the stability of the system. In fact, after the hydrogen dissociates to the O_{3c}, the distance between the corresponding O_{3c} and the nearby Ce also increases significantly, causing destruction of the CeO₄ unit (Figure 6a).

It needs to be noted that although the ammonia dissociation to the O_{2c} is more stable than O_{3c}, the ammonia adsorbed on the surface is relatively far away from the O_{2c}, which makes the direct dissociation process to be kinetically unfavorable. Thus, the ammonia is most likely to dissociate the hydrogen first to the adjacent O_{3c} (Figure 6a), and then the hydrogen migrates from the O_{3c} to the O_{2c} (Figure 6b).

The further dissociation of NH₂ species was also considered, and the calculated results showed that the dissociation of the NH₂ species to transfer the H to either the O_{2c} or the O_{3c} is endothermic by 0.54 eV and 1.07 eV, respectively. In particular, the process of NH₂ dissociation to O_{3c} is a highly endothermic process, which indicates the high activation energy of the dissociation. Therefore, the NH₂ species is hard to dissociate and it could be the main dissociated product of ammonia on the surface.

the dissociation of NH_2 and it also promotes the break of N–H bond.

Oxygen vacancy will be backfilled by the absorbed oxygen. However, the adsorbed oxygen on the surface is far away from the oxygen vacancy. Thus, before the oxygen molecule backfills the oxygen vacancy, the migration of the oxygen vacancy first occurs to reduce the distance between the absorbed oxygen and the oxygen vacancy. The migration of oxygen vacancy is complex and may involve the migration of the lattice oxygen in surface and bulk phase. Nevertheless, the net result is the migration of oxygen vacancy on the side of HNO species to the side of absorbed O_2 (Figure 8d).

The calculated results showed that the migration of oxygen vacancies is exothermic by 0.11 eV, indicating that oxygen vacancies are more stable on the side of oxygen and the migration is thermodynamically favorable. After the migration of the oxygen vacancy to the side of Ce site with the adsorbed oxygen, the bond length of the oxygen molecule slightly increases from 1.339 Å to 1.349 Å, and it also slightly tilted toward the oxygen vacancy.

The oxygen molecule will then adsorb in the oxygen vacancy before it is backfilled (Figure 8e). The oxygen molecule adsorption in the oxygen vacancy is further exothermic by 0.11 eV, and the O–O bond length increases to 1.381 Å. The dissociation of the oxygen molecule adsorbed in the oxygen vacancy (Figure 8f) is strongly exothermic by 0.96 eV. When the oxygen molecule dissociates and backfills the oxygen vacancy with one oxygen atom, the remaining oxygen atom is adsorbed on top of the Ce sites, and the Ce–O distance is significantly shortened to 1.922 Å.

NO is mainly produced by dehydrogenation of HNO. For this process, we considered it to be similar to the dissociation of ammonia described above, where the hydrogen first leaves to the relatively closer O_{3c} (Figure 8g), and then further migrates to the O_{2c} (Figure 8h).

The dehydrogenation of HNO to the neighboring O_{3c} is strongly exothermic by 1.13 eV. When HNO is dehydrogenated, the N–O bond length is significantly shortened from 1.292 Å to 1.188 Å. The further migration of the hydrogen from the O_{3c} to the O_{2c} is also exothermic by 0.64 eV. These results indicated that the dehydrogenation of HNO species is thermodynamically favorable.

The transition state of each above step was also determined and shown in Figure 9. The calculated energy profiles and the key states of the oxidation processes were shown in Figure S2. The results suggested that the formation of NH_2O has the highest energy barrier during the whole process, which may be the rate-determining step.

Conclusions

In this work, we conducted the DFT+U study to investigate the ammonia oxidation process on the $\text{Cu}_1/\text{CeO}_4\text{-t-p}$ surface. The major conclusions are summarized as follows.

After the single-atom copper loading on the $\text{CeO}_4\text{-t-p}$ surface, the copper atom will lose an electron and one of the Ce in the surface CeO_4 unit will store the electron and be reduced to Ce^{3+} . The stored electron will transfer to one oxygen molecule to promote its adsorption on the Ce site. Both oxygen and ammonia tend to adsorb on the Ce site of the $\text{Cu}_1/\text{CeO}_4\text{-t-p}$ surface and can co-adsorb on two different Ce sites simultaneously.

The dissociation of ammonia on the catalyst surface is assisted by lattice oxygen. The ammonia can dissociate to leave the H

to the surface O_{2c} with low energy barrier. This dissociation process to form NH_2 species on the catalyst surface is exothermic. The further dissociation of NH_2 species to form NH species is endothermic and unlikely to occur.

The NH_2 species can be further oxidized by a lattice oxygen to form the NH_2O species with the formation of an oxygen vacancy. The formation of NH_2O species can promote the breaking of N–H bond to form the HNO species. The oxygen vacancy will migrate and be backfilled by oxygen molecules adsorbed on the surface Ce sites. So, the ammonia oxidation on this catalyst actually follows the Mars–van Krevelen mechanism. The further dehydrogenation of HNO species will generate NO. The formation of NH_2O species has the highest activation energy, which indicates it may be the rate determination step of the whole process. Finally, the NO might be able to react with other NH_3 adsorbed on the surface to form N_2 .

Supporting Information

The following supporting information can be downloaded at:
<https://global-sci.com/storage/self-storage/cicc-2025-43-1-r1-si.pdf>

Acknowledgement

This work was supported by the National Key R & D Program of China (2024YFA1509901).

References

- [1] Grabchenko M. V., Mamontov G. V., Zaikovskii V. I., La Parola V., Liotta L. F., Vodyankina O. V. The role of metal–support interaction in Ag/CeO_2 catalysts for CO and soot oxidation. *Appl. Catal. B-Environ.*, **260** (2020) 118148.
- [2] Liu H. X., Li S. Q., Wang W. W., Yu W. Z., Zhang W. J., Ma C., Jia C. J. Partially sintered copper–ceria as excellent catalyst for the high-temperature reverse water gas shift reaction. *Nat. Commun.*, **13** (2022) 867.
- [3] Li H. Y., Wang H. F., Gong X. Q., Guo Y. L., Guo Y., Lu G., Hu P. Multiple configurations of the two excess 4f electrons on defective CeO_2 (111): Origin and implications. *Phys. Rev. B*, **79** (2009) 193401.
- [4] Zhou K., Wang X., Sun X., Peng Q., Li Y. Enhanced catalytic activity of ceria nanorods from well-defined reactive crystal planes. *J. Catal.*, **229** (2005) 206–212.
- [5] Mai H. X., Sun L. D., Zhang Y. W., Si R., Feng W., Zhang H. P., Liu H. C., Yan C. H. Shape-selective synthesis and oxygen storage behavior of ceria nanopolyhedra, nanorods, and nanocubes. *J. Phys. Chem. B*, **109** (2005) 24380–24385.
- [6] Lin Y., Wu Z., Wen J., Poeppelmeier K. R., Marks L. D. Imaging the atomic surface structures of CeO_2 nanoparticles. *Nano Lett.*, **14** (2014) 191–196.
- [7] Capdevila-Cortada M., López N. Entropic contributions enhance polarity compensation for CeO_2 (100) surfaces. *Nat. Mater.*, **16** (2017) 328–334.
- [8] Zhou H., Wu X., Gong X. Structural shrinking and rotation decrease quasi surface tension for polar CeO_2 (100). *Adv. Theor. Simul.*, **5** (2022) 2200081.
- [9] Valera-Medina A., Xiao H., Owen-Jones M., David W. I. F., Bowen P. J. Ammonia for power. *Prog. Energy. Combust.*, **69** (2018) 63–102.
- [10] Chai W. S., Bao Y., Jin P., Tang G., Zhou L. A review on ammonia, ammonia-hydrogen and ammonia-methane fuels. *Renew. Sust. Energy. Rev.*, **147** (2021) 111254.

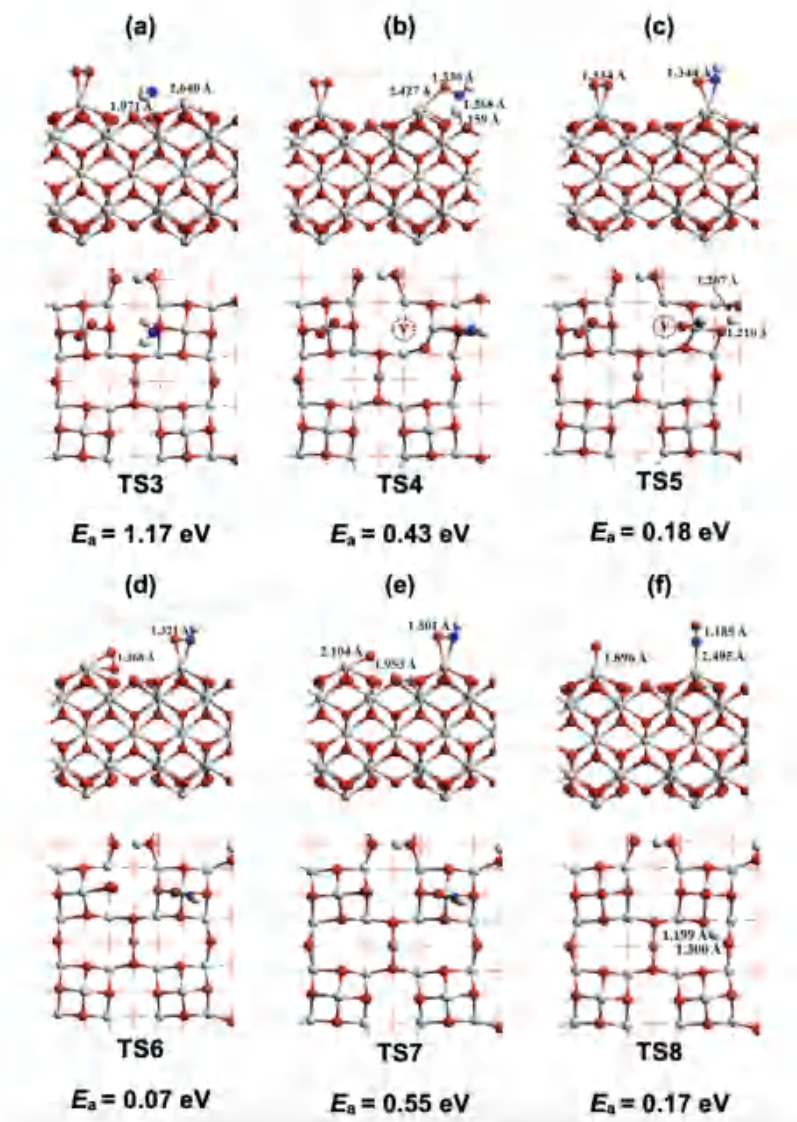


Figure 9. Calculated transition states and activation energies of (a) NH_2O formation, (b) dissociation of NH_2O , (c) hydrogen migration, (d) adsorption of oxygen in oxygen vacancy, (e) oxygen dissociation and backfill of the oxygen vacancy, (f) NHO dissociation, and (g) hydrogen migration.

- [11] Erdemir D., Dincer I. A perspective on the use of ammonia as a clean fuel: Challenges and solutions. *Int. J. Energ. Res.*, **45** (2021) 4827–4834.
- [12] Wang B., Fu Y., Xu F., Lai C., Zhang M., Li L., Liu S., Yan H., Zhou X., Huo X., Ma D., Wang N., Hu X., Fan X., Sun H. Copper single-atom catalysts—a rising star for energy conversion and environmental purification: Synthesis, modification, and advanced applications. *Small* **2023** 2306621.
- [13] Rabee A. I. M., Abed H., Vuong T. H., Bartling S., Krauß L., Atia H., Rockstroh N., Kondratenko E. V., Brückner A., Rabeah J. CeO_2 -supported single-atom Cu catalysts modified with Fe for RWGS reaction: Deciphering the role of Fe in the reaction mechanism by in situ/operando spectroscopic techniques. *ACS Catal.*, **14** (2024) 10913–10927.
- [14] Huang F., Chen X., Sun H., Zeng Q., Ma J., Wei D., Zhu J., Chen Z., Liang T., Yin X., Liu X., Xu J., He H. Atmosphere induces tunable oxygen vacancies to stabilize single-atom copper in ceria for robust electrocatalytic CO_2 reduction to CH_4 . *Angew. Chem. Int. Ed.*, **64** (2025) e202415642.
- [15] Kresse G., Hafner J. *Ab initio* molecular dynamics for open-shell transition metals. *Phys. Rev. B* **48** (1993) 13115–13118.
- [16] Perdew J. P., Burke K., Ernzerhof M. Generalized gradient approximation made simple. *Phys. Rev. Lett.*, **77** (1996) 3865–3868.
- [17] Blöchl P. E. Projector augmented-wave method. *Phys. Rev. B*, **50** (1994) 17953–17979.
- [18] Alavi A., Hu P., Deutsch T., Silvestrelli P. L., Hutter J. CO oxidation on Pt(111): An *ab initio* density functional theory study. *Phys. Rev. Lett.*, **80** (1998) 3650–3653.

- [19] Kummerle E. A., Heger G. The structures of $\text{C-Ce}_2\text{O}_{3+\delta}$, Ce_7O_{12} , and $\text{Ce}_{11}\text{O}_{20}$. *J. Solid State Chem.*, **147** (1999) 485–500.
- [20] Zhou C. Y., Wang D., Gong X. Q. A DFT+U revisit of reconstructed CeO_2 (100) surfaces: Structures, thermostabilities and reactivities. *Phys. Chem. Chem. Phys.*, **21** (2019) 19987–19994.
- [21] Hinokuma S., Shimanoe H., Matsuki S., Kawano M., Kawabata Y., Machida M. Catalytic activity and selectivities of metal oxides and $\text{Pt/Al}_2\text{O}_3$ for NH_3 combustion. *Chem. Lett.*, **45** (2016) 179–181.
- [22] Choi Y. M., Abernathy H., Chen H., Lin M. C., Liu M. Characterization of O_2 – CeO_2 interactions using in situ Raman spectroscopy and first-principle calculations. *ChemPhysChem*, **7** (2006) 1957–1963.
- [23] Miller J. A., Smooke M. D., Green R. M., Kee R. J. Kinetic modeling of the oxidation of ammonia in flames. *Combust. Sci. Technol.*, **34** (1983) 149–176.